



Gross primary productivity of forest ecosystems in a subtropical city and its decadal climatic and environmental drivers

Hayden C. H. Lam¹, David H. Y. Yung¹, Donald K. C. Tao¹, Joshua T. W. Lo^{1,2}, Man Sing Wong^{3,4}, Jin Wu^{5,6,7}, and Amos P. K. Tai^{1,7,8}

Correspondence: Amos P. K. Tai (amostai@cuhk.edu.hk)

Abstract. Vegetation plays a vital role in modulating climate and the carbon cycle on land through processes like photosynthesis, also known as gross primary production (GPP). The significant presence of vegetation in Hong Kong, covering over 70 % of the land area, highlights the potential for terrestrial carbon sink to contribute to achieving carbon neutrality in such a metropolitan city. Meanwhile, the terrestrial ecosystem is also influenced by climatic and environmental factors. This study investigates the historical spatiotemporal dynamics of GPP in the subtropical forests of Hong Kong and the key drivers behind its trend and interannual variability between 2002 and 2018. We used the Terrestrial Ecosystem Model in R-Hong Kong (TEMIR-HK), a localized process-based ecophysiological model, to evaluate the changes in GPP induced by changing CO₂ concentration, temperature, ozone (O₃) concentration, and changing leaf area index (LAI) shaped by these factors as well as land use. Simulation results indicate an increasing trend of GPP, with an average annual GPP of 1.75 TgC yr⁻¹, which is around 15 % of the annual total anthropogenic carbon emission from Hong Kong, suggesting a limited but indispensable potential of forestry to achieve city-level carbon neutrality. Model simulations of GPP show satisfactory results when spatially comparing with satellite-based GPP dataset (R = 0.89), with slight difference of +8.7 % on average. Factorial simulations reveal LAI changes dominate both trend (+0.0134 TgC yr⁻²) and interannual variability (standard deviation: 2.77×10⁻² TgC m⁻² yr⁻¹) of GPP in Hong Kong. This result highlights that local-scale reforestation could influence GPP trend over the whole city and emphasizes the importance on the accuracy of LAI input in ecosystem-scale photosynthesis modelling. This work contributes to improving the scientific understanding on subtropical forest ecosystems, and highlights the potential, though limited, of Hong Kong forests to play their parts in working toward carbon neutrality targets.

¹Department of Earth and Environmental Sciences, Faculty of Science, The Chinese University of Hong Kong, Shatin, Hong Kong

²Flora Conservation Department, Kadoorie Farm and Botanic Garden, Tai Po, Hong Kong

³Department of Land Surveying and Geo-Informatics, The Hong Kong Polytechnic University, Hung Hom, Hong Kong

⁴Research Institute for Land and Space, The Hong Kong Polytechnic University, Hung Hom, Hong Kong

⁵Research Area of Ecology and Biodiversity, School of Biological Sciences, The University of Hong Kong, Pok Fu Lam, Hong Kong

⁶Institute for Climate and Carbon Neutrality, The University of Hong Kong, Pok Fu Lam, Hong Kong

⁷State Key Laboratory of Agrobiotechnology, The Chinese University of Hong Kong, Shatin, Hong Kong

⁸Institute of Environment, Energy and Sustainability, The Chinese University of Hong Kong, Shatin, Hong Kong



35



1 Introduction

The exchange of energy, water, carbon and other climatically relevant elements are vastly regulated by plants through photosynthesis, which provides the largest sink for atmospheric carbon and represents the largest carbon flux in the terrestrial carbon cycle. Gross primary productivity (GPP), defined as the total amount of energy captured by autotrophs through photosynthesis, is a key regulator of climate, and provides the basis for the functioning of matter and energy transfer in ecosystems. It is also a proxy for studying terrestrial carbon sequestration. It is estimated that the terrestrial carbon sink could offset 31 % of global total anthropogenic CO₂ emissions during 2013–2022 (Friedlingstein et al., 2023). Not only does GPP reflect the productivity of an ecosystem, but it also affects the carbon stocks of biomass and regional climate through altering transpiration and evaporative cooling. Meanwhile, the terrestrial biosphere is also continuously transformed by the changing climate and environment. More accurately quantifying GPP, its variability and driving factors is hence pivotal in understanding the terrestrial carbon cycle and its effects on climate change (Ryu et al., 2019).

GPP responds to meteorological and environmental factors in both direct and indirect ways. Enzymatically, photosynthesis increases with increasing atmospheric CO₂ concentration ([CO₂]) following a Michaelis-Menton curve. Elevated [CO₂] from 366 to 567 ppm was reported to stimulate light-saturated photosynthesis for C3 plants by an average of 31 % in free-air CO₂ enrichment (FACE) experiments (Ainsworth and Rogers, 2007). By partitioning the net carbon sink into different regions and comparing process-based and atmospheric inverse model outputs, Schimel et al. (2015) showed that the CO₂ fertilization feedback contributes to 2.5 PgC yr⁻¹ of terrestrial carbon uptake, which is 60 % of the total present-day land sink.

Temperature has been shown to be a dominant factor controlling photosynthetic activity (e.g., Berry and Bjorkman, 1980; Fernández-Martínez et al., 2018; Hikosaka et al., 2006; Li et al., 2015, 2016; Wu et al., 2011). It is well established that the temperature response curve of leaf photosynthesis follows a parabolic shape: photosynthesis rate increases with temperature until an optimum temperature is reached, and then declines with even higher temperature (Berry and Bjorkman, 1980; Lloyd and Farquhar, 2008). Above the optimum temperature, net photosynthesis rate is co-limited by Rubisco deactivation and chloroplast electron transport rates (Scafaro et al., 2023). At the ecosystem level, elevated air temperature further influences photosynthesis through controlling vapour pressure deficit (Park Williams et al., 2012). Twine and Kucharik (2009) suggested that in the US, 19 % of corn and 11 % of soybean net primary productivity (NPP) trends could be attributable to temperature trends. Global warming in general stimulates ecosystem photosynthesis by an average of 20 %, and ecosystem photosynthesis shows significantly positive sensitivity to warming in a meta-analysis (Wu et al., 2011). In China, 1–2 °C increment in temperature has stimulated an accelerating trend in net productivity, while >2 °C warming decreases the positive trend (Gu et al., 2017).

Tropospheric ozone (O_3) induces substantial damage to vegetation via stomatal uptake. High O_3 exposure causes rapid transient reduction in stomatal conductance, which could be recovered within a short period of time (Vahisalu et al., 2010). Chronic O_3 exposure has been shown to reduce stomatal conductance and thus photosynthesis and transpiration irreversibly, altering the carbon and water cycles (Lombardozzi et al., 2015). The indirect climate forcing of reduced carbon sink by O_3 deposition could be larger than the direct radiative forcing of O_3 as a greenhouse gas (GHG) (Sitch et al., 2007). Collecting



55



observations over 1900 trees worldwide, Wittig et al. (2007) estimated the elevated O_3 concentration ($[O_3]$) since industrial revolution has hindered tree photosynthesis by 11 %. A mechanistic model projected a 14–23 % reduction in GPP over the period 1901–2100 due to rising O_3 pollution (Sitch et al., 2007).

There are interplays between $[CO_2]$, temperature and $[O_3]$ that may provide synergistic or counteractive effects on photosynthesis, mainly through modulating the stomata. Elevated $[CO_2]$ would lead to reduction in stomatal conductance, which in turn reduces O_3 dry deposition and alleviates O_3 damage, constituting a protective effect. On the other hand, reduced O_3 deposition may result in higher ambient $[O_3]$. FACE experiments have shown that elevated $[CO_2]$ might not be able to offset the O_3 damage entirely (Uddling et al., 2010). In order to balance the conflicting needs of vegetation between carbon gain and water loss prevention, increasing stomatal closure can happen under elevated $[CO_2]$ as well as increasing water stress induced by warming (Lloyd and Farquhar, 2008; Medlyn et al., 2011).

The indirect impacts on photosynthesis induced by climatic and environmental factors and direct human factors also manifest through alterations in canopy structure. The total indirect environmental effects on GPP through altering canopy structure could be comparable to the direct effect (Chen et al., 2023b). One of the indicators of canopy structure, leaf area index (LAI), has been widely adopted in the studies of vegetation productivity and vegetation responses to climate change (Chen et al., 2023a, b; Winkler et al., 2021; Zhu et al., 2016). The said CO₂ fertilization effects on GPP can result in an expansion in leaf area (Donohue et al., 2013) and drive the globally observed greening trends (Zhu et al., 2016). Warming is also suggested to promote earlier spring phenology (higher LAI in spring) and induce an increase in carbon uptake (Gu et al., 2022), while vegetation management and disturbances influence regional greening. Forests and croplands exhibit significant greening trends and human land-use management accounts for at least one-third of the observed net increase in leaf area predominantly in China and India (Chen et al., 2019). Meanwhile, insect outbreaks and diseases associated with the warming trends could also contribute to the browning trend in North American boreal forests (Verbyla, 2011).

Subtropical forests that lie within the transition zone between tropical and temperate forests, such as those in the city of Hong Kong in South China, are less well studied than tropical or temperate ones. Similar to tropical forests, subtropical forests are mostly composed of evergreen species, with underlying canopies of shrubs and grasses. Subtropical forests could maintain high level of photosynthetic activity throughout the year, even in cold winters (Requena Suarez et al., 2019; Tan et al., 2012). Leaf photosynthesis generally increases with temperature in subtropical vegetation without reaching the high temperature threshold, despite variation in species-specific responses (Li et al., 2016). In the context of forest dynamics, a subtropical large-scale biodiversity experiment showed that an accumulation of carbon in a 16-species mixture is twice the amount found in average monocultures in an 8-year period (Huang et al., 2018). Subtropical forests have their unique behaviours and large photosynthetic potential that are worthwhile for further studies.

The uniqueness of Hong Kong as a subtropical city provides important reference for city-scale land carbon sink. Despite the fact that it is a highly developed coastal city, more than 70 % of the land is covered by vegetation. There are ~700,000 urban trees and ~550 species, and 24 country parks covering ~40 % of total land area (Agriculture, Fisheries and Conservation Department, 2023). Hong Kong's flora is generically tropical, but less so when compared with places near the equator (Dudgeon and Corlett, 1994). The extensive and diverse vegetation in Hong Kong has provided the potential of significant contribution





of terrestrial carbon sink in achieving carbon neutrality for the city. Studying ecosystem GPP is the cornerstone in studying ecosystem services provided by Hong Kong vegetation.

Different approaches have been applied to study the terrestrial ecosystem productivity in Hong Kong. Site-level carbon sequestration of mangrove wetlands and urban turfgrasses was studied in Hong Kong (Kong et al., 2014; Liu and Lai, 2019). A process-based biochemical model for mangrove was developed and calibrated with site observations whereby one out of the two eddy covariance flux measurement sites is located in the mangrove ecosystem in Hong Kong (Tang et al., 2023). Chan et al. (2021) estimated aboveground biomass at various plot sizes using regression models based on data from the Light Detection and Ranging (LiDAR) instrument. Using global terrestrial biosphere models (TBMs), Cui et al. (2019) simulated an ensemble mean gross GPP of 1280 ±422 gC m⁻² yr⁻¹ during 1901–2010 in the East Asian Monsoon region, of which Hong Kong is a part, and subtropical evergreen forests and croplands show greater intermodel disagreement in GPP. To date, there is no study specifically focusing on the long-term GPP dynamics of Hong Kong forests. Local studies relying on emission factor, allometric methods and flux tower observations were either limited to a plot scale (Kong et al., 2014; Liu and Lai, 2019) or a specific plant type (Lee et al., 2021; Tang et al., 2023). TBMs could produce regional gridded results (Cui et al., 2019), but global models have a very coarse spatial resolution (0.5°×0.5°) that does not enable fine-scale characterization of Hong Kong's forests.

Here we thus aim to estimate the total gross carbon uptake by vegetation in the whole city of Hong Kong, and investigate the major drivers of GPP under the combination of subtropical climate and forest management. This is the first comprehensive study on the temporal dynamics of GPP in Hong Kong and the climatic and environmental factors controlling its changes. It is also the first process-based modelling study on vegetation productivity over the entire Hong Kong region at a fine spatial resolution across different existing vegetation types, allowing computational factorial experiments to decipher the driving factors. By understanding the contribution of subtropical forest ecosystems to local terrestrial carbon sink, and its climatic and environmental driving factors, our results provide decision support for tree planting strategies and management, especially as the city aims to achieve carbon neutrality by multiple means.

110 2 Methodology

100

105

This study consists of two major components. First, we examined the observed GPP trend and interannual variability (IAV) and investigated how well the model simulations reproduce the observations. Second, we conducted and analysed the factorial simulations to disentangle the effects of the aforementioned drivers and determined their relative roles (Pan et al., 2014).

2.1 Study area

Located at 22.3964° N, 114.1095° E in the coastal area, Hong Kong can be divided into three major geographical regions: Hong Kong Island, Kowloon and the New Territories (comprising the Lantau Island and other outlying islands). In this study, we separated the New Territories and the Lantau Island to avoid ambiguity. In between the varying topography composed of numerous islands and mountains with a land area of 1104 km² lives a human population of more than 7 millions (Lands



125



Department, 2024). Hong Kong has a subtropical monsoon climate. In winter, cool and dry air is brought by the northerly or northeasterly winds, while in summer, warmer and moister air is brought from the tropical oceans (Dudgeon and Corlett, 1994). Hong Kong exhibits large temperature seasonality, ranging from a daily mean of 17 °C in January to 32 °C in July (https://www.hko.gov.hk/en/cis/climahk.htm, last access: 4 January 2025). The mean daily temperature (1994–2023) is 23.7 °C, and the annual total rainfall is 2452 mm. The existing vegetation is mainly secondary forests planted in the latter half of the 20th century after the Second World War. In the early years, exotic species were planted to prevent soil erosion and restore vegetation cover destroyed by fires. These species have been gradually removed and replanted with native tree seedlings to enhance ecological values under the Country Parks Plantation Enrichment Programme (PEP) initiated by the Agriculture, Fisheries and Conservation Department (AFCD) in recent years (Agriculture, Fisheries and Conservation Department, 2023). The major types of vegetation are woodlands, shrublands and grasslands.

2.2 Process-based model description

TEMIR-HK computes ecophysiological processes including photosynthesis, stomatal conductance and dry deposition in instantaneous response to changing weather, atmospheric composition and land environment. Originated from the Terrestrial Ecosystem Model in R version 1.0 (TEMIR v1.0) (Tai et al., 2024), TEMIR-HK adopts the same schemes as TEMIR, but allows finer spatial resolution (0.005°×0.005°) and localized inputs (Tao, 2021). TEMIR-HK simulates hourly gridded gross canopy photosynthesis for 24 plant functional types (PFTs). Figure 1 describes a simplified model simulation workflow in TEMIR-HK. In the radiative transfer model, direct and diffuse radiation are used to calculate the absorbed photosynthetically 135 active radiation (PAR) by sunlit and shaded leaves, following a single "big-leaf" approach. Leaf photosynthesis then follows the well-established enzyme kinetic formulations, which consider the three limiting regimes of photosynthesis that require PFT-specific physiological parameters and intercellular CO₂ concentration (see Table S2 from (Tai et al., 2024)). Using leaf photosynthesis and atmospheric conditions such as water vapour pressure, the stomatal conductance of water can be calculated. Subsequently, O₃ damages on leaf photosynthesis and stomatal conductance are represented by an O₃ damage factor that relies 140 on leaf boundary layer conductance, aerodynamic conductance and ambient O₃ concentration. Sunlit and shaded leaf area indices obtained in the radiative transfer model are then multiplied to the leaf photosynthesis to upscale to canopy level outputs. Detailed description of the model can be found in Tai et al. (2024).

2.3 Data sources

150

45 **2.3.1** Plant functional types

We adopted the 30-m resolution Global Land Cover 2015 dataset in the Finer Resolution Observation System and Monitoring of Global Land Cover (FROM-GLC) land classification system (hereafter "FROM-GLC 2015") (Gong et al., 2012; Li et al., 2017) as the default land cover type. The data product was trained using Random Forest algorithm and validated with Landsat-8 data (Li et al., 2017). FROM-GLC 2015 is the only land cover type dataset with a high resolution of 30 m, which enables the computation of PFT fractions for each of our model grid cells of 500 m. PFTs are aggregated plant species





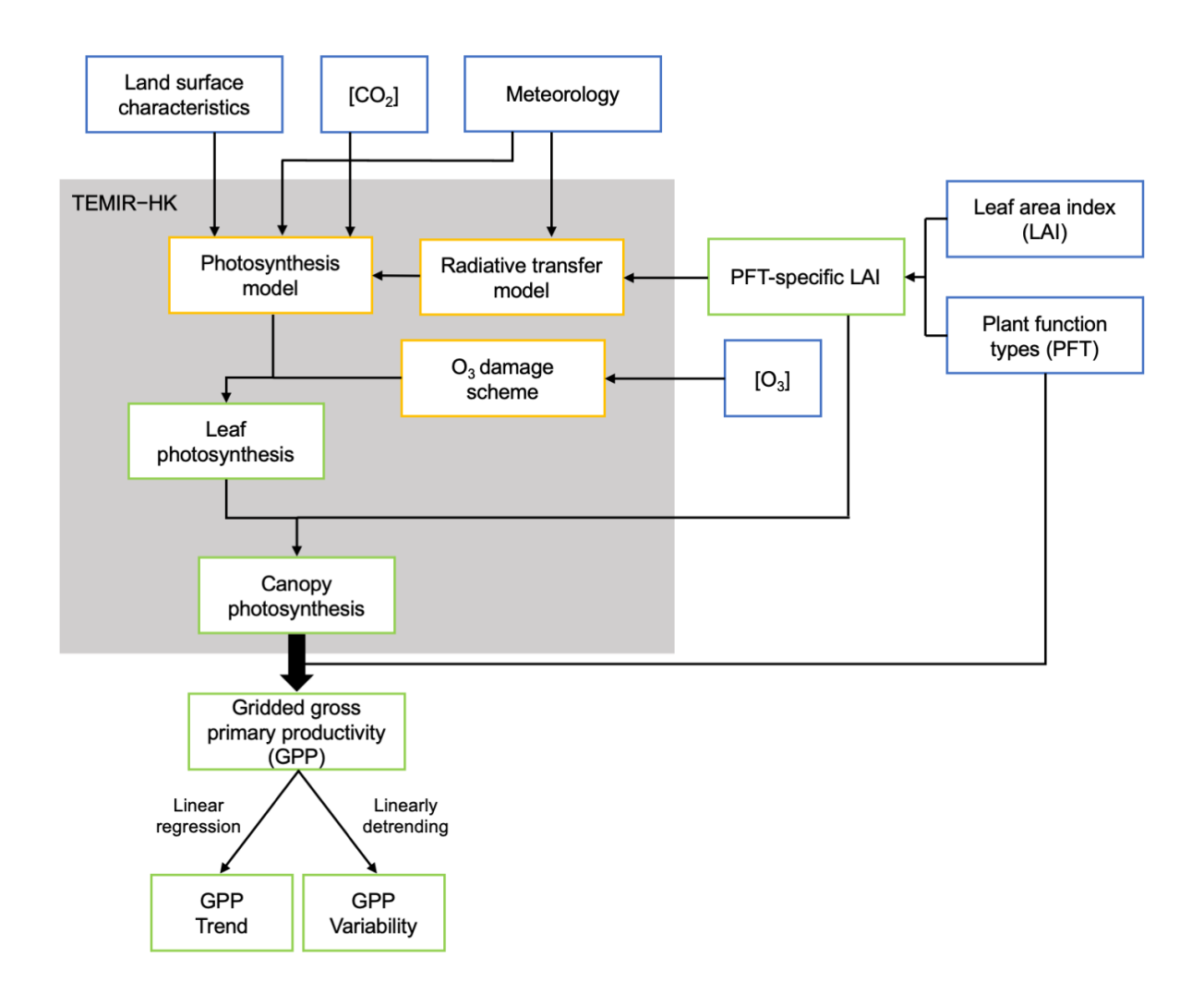


Figure 1. Methodological workflow of this study. TEMIR-HK computes canopy gross primary productivity (GPP) driven by meteorological and environmental factors. The gridded GPP is further decomposed into trend and variability by linear regression.

categories based on biophysical properties and functions. They enable a parameterization that represents each model grid cell as a mosaic of vegetation, and do not necessarily correspond to genetic categorization. The 24 Level-2 classes of land cover types abundant in Hong Kong were translated into PFT fractions using a cross-walking table (Table S1) modified from Reinhart et al. (2022). The cross-walking table is based on Holdridge Life Zones—biotemperature and precipitation. We determined the Holdridge Life Zone in Hong Kong using temperature and precipitation data from the Hong Kong Observatory (https://www.hko.gov.hk/en/wxinfo/pastwx/mws/mws.htm, last access: 11 June 2025), and modified the PFTs according to our understanding to local plant species. The translated PFT map was rescaled to 500 m resolution and parameterized into PFT fractions for model simulation as illustrated in Fig. 2. There are six abundant PFTs in Hong Kong. The relative abundances of PFTs are listed here in descending order: broadleaf evergreen tropical tree (BETT), 34.0 %; broadleaf evergreen shrub (BES),





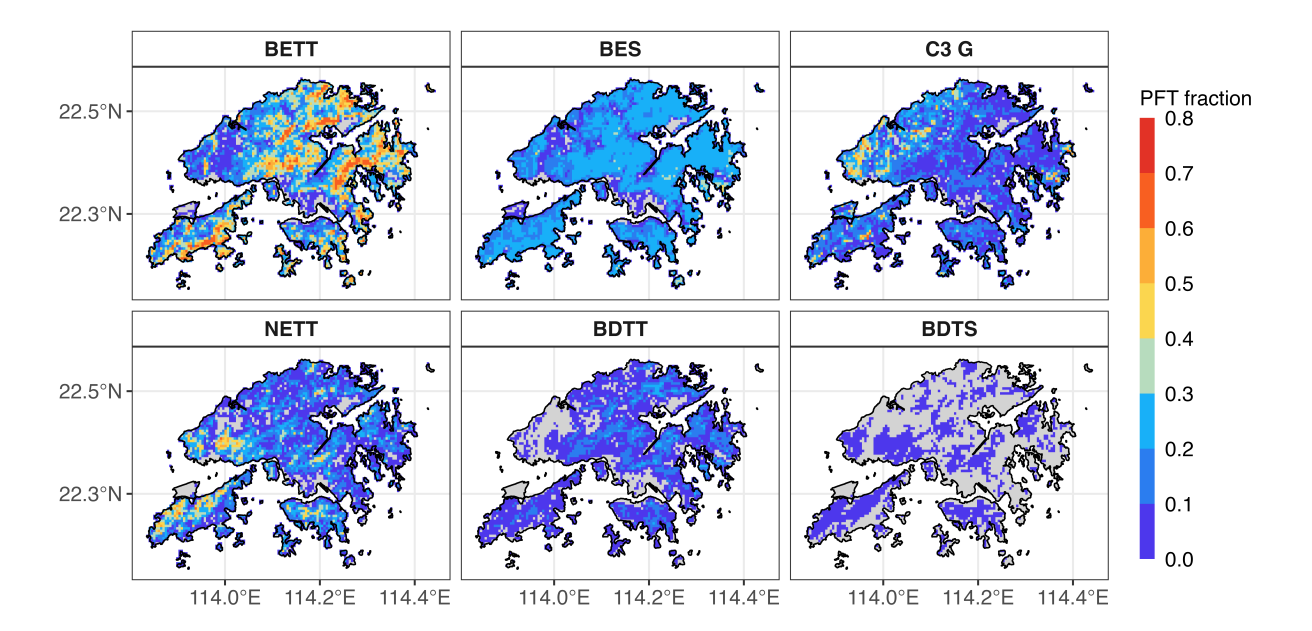


Figure 2. Rescaled 500 m resolution plant functional type (PFT) fractions derived from 30 m resolution Global Land Cover 2015 dataset in the Finer Resolution Observation System and Monitoring of Global Land Cover (FROM-GLC) for (a) broadleaf evergreen tropical tree (BETT), (b) broadleaf evergreen shrub (BES), (c) C3 grass (C3 G), (d) needleleaf evergreen tropical tree (NETT), (e) broadleaf deciduous temperate tree (BDTT) and (f) broadleaf deciduous temperate shrub (BDTS) in Hong Kong.

23.5 %; C3 non-arctic grass (C3 G), 17.2 %, needleleaf evergreen temperate tree (NETT), 16.9 %; broadleaf deciduous tropical tree (BDTT), 7.2 %; broadleaf deciduous temperate shrub (BDTS), 1.2 %.

2.3.2 Leaf area index

We adopted MODIS MCD15A3H v006 4-day composite LAI data product with 500 m resolution. Daily LAI values were linearly interpolated from the dataset. As TEMIR-HK requires PFT-specific LAI for each model grid cell, the dataset was further processed to be PFT-specific using current day PFT fraction (PFT frac) and a PFT-specific LAI from a base year (LAI_{base,PFT}) (Figure 1). This approach allocates the current day total LAI of the grid cells to different PFTs based on the PFT fractions. A scaling factor for each grid, *Z*, is calculated as:

$$Z = \frac{\text{LAI}}{\Sigma(\text{LAI}_{\text{base}, PFT} \times \text{PFT frac})}$$
 (1)

The current-day PFT-specific LAI is thus

$$170 \quad LAI_{PFT} = Z \times LAI_{base, PFT}$$
 (2)



180

185

190



Table 1. Factorial case setup for the simulations. "Full" refers to temporally fully changing, and "Fixed" refers to the fixed mean of 2010–2012. The fixed cases are fixing atmospheric [CO₂], temperature, ambient [O₃] and leaf area index (LAI) respectively.

	Variable			
Case	[CO ₂]	Temperature	$[O_3]$	LAI
⟨Full⟩	Full	Full	Full	Full
⟨CO2_fixed⟩	Fixed	Full	Full	Full
⟨Temp_fixed⟩	Full	Fixed	Full	Full
⟨O3_fixed⟩	Full	Full	Fixed	Full
(LAI_fixed)	Full	Full	Full	Fixed

2.3.3 Meteorological and environmental data

We used eight locally measured meteorological variables, namely surface air temperature, wind speed, precipitation, relative humidity, sea level pressure, and diffuse, direct and global solar radiation. We adopted hourly meteorological data measured at over 78 ground monitoring stations of the Hong Kong Observatory (HKO) and hourly ozone concentration ([O₃]) from eight air quality monitoring stations of the Hong Kong Environmental Protection Department (HKEPD). These observed variables were extrapolated to gridded data by inverse distance weighting interpolation approach with a power parameter of 2 (Lu and Wong, 2008). For missing data and other required meteorological variables such as surface energy fluxes, we used the reanalysis products of Modern-Era Retrospective analysis for Research and Applications, Version 2 (MERRA-2) within the designated study period. For land surface information and soil parameters, including soil moisture and vertical root fraction, we represented them by a surface data map from the Community Land Model 2 (CLM2). Yearly ambient [CO₂] in Hong Kong was extracted from global monthly gridded atmospheric [CO₂] data produced by Cheng et al. (2022). The data was spatially reconstructed based on Climate Model Intercomparison Project 6 (CMIP6) outputs and emission data. We adopted the SSP2-4.5 scenario for 2015–2018 in this study. For the gap year 2014 in the dataset that separates the historical [CO₂] and the future projection, we linearly interpolated the concentration using the available data in 2004–2013 and 2015–2018.

2.3.4 Satellite-based GPP data

We used Moderate Resolution Imaging Spectroradiometer (MODIS) MOD17A2HGF Version 6.1 GPP product (hereafter "MODIS GPP") as the proxy dataset for observation-model comparison. The data product is a cumulative 8-day composite of values with a resolution of 500 m, based on the radiation use efficiency concept that utilizes photosynthetically active radiation and climate variables. The GPP data for 2004–2018 were remapped to be consistent with the spatial extent of TEMIR-HK and aggregated to annual mean for comparison.



200

205

215



2.4 Experimental setup

Five factorial simulations were conducted with TEMIR-HK with various combinations of meteorological and environmental factors. The proposed key drivers of GPP: [CO₂], temperature, [O₃] and LAI (hereafter "proposed drivers"), were fixed specifically for the fixed-factor simulations (see Table 1). We acknowledge that LAI is inherently shaped by the climatic and environmental factors as mentioned in the introduction; however, since the model considers prescribed LAI input, here it is treated as a quasi-independent factor for the purpose of factorial experiments. We therefore essentially aimed to explore whether using transient LAI would bring significant changes to the model results. For the fixed variables, we used the yearly/daily/hourly mean (depending on the model requirement) of the middle three years of the study period, i.e., 2010–2012. Here we define the first simulation as the one with all the proposed drivers remain temporally changing (hereafter "full case"). The remaining 4 simulations are the "fixed cases" in which one of the proposed drivers is fixed for each case (Table 1). The effect on simulated GPP by an individual proposed driver could be isolated by the subtraction of the fixed case from the full case, assuming the effects by the proposed drivers are additive (Franz and Zaehle, 2021). There are two choices of O₃ damage scheme: "Sitch scheme" that follows Sitch et al. (2007) and "Lombardozzi scheme" that follows Lombardozzi et al. (2012, 2015). We used the "Sitch scheme" with "high" O₃ sensitivity that does not require model spin-up for all simulations. Under "high" O₃ sensitivity, plants especially C3 grasses, tend to be more vulnerable to O₃ damage when compared to "low" O₃ sensitivity.

2.5 Model output processing and analysis

We used the output gridded PFT-specific GPP (per unit area) and PFT fractions to calculate regional total GPP in Hong Kong.

$$GPP_{total} = \sum_{1}^{m} \left[\sum_{1}^{n} (GPP_{m,n} \times PFT \operatorname{frac}_{m,n}) \times \operatorname{Area}_{m} \right]$$
(3)

where GPP_{total} is the regional total GPP, GPP_{m,n} is the gridded PFT-specific GPP, PFT frac_{m,n} is the gridded PFT fraction, 210 Area_m is the area for each grid, and m, n are the total number of grids and PFTs respectively.

For trend analysis, we used non-parametric Mann-Kendall trend test (hereafter "M-K test") to test whether a temporal trend is statistically significant for a quantity. We applied linear regression to gridded yearly GPP and total GPP to obtain the trends to examine their time evolution. At the same time the interannual variability of GPP could also be obtained by removing the trend. Here we used annual standard deviations of the detrended GPP to indicate the interannual variability (hereafter "IAV") of GPP.

3 Results and discussion

3.1 Spatiotemporal dynamics of GPP

We first describe the spatiotemporal dynamics of GPP in Hong Kong with the observed MODIS GPP. Mean annual GPP during 2004–2018 over Hong Kong is 1.46 ± 0.06 TgC yr⁻¹. Figure 3a shows the spatial GPP distribution in Hong Kong. High levels of GPP (2.4–3.0 kgC m⁻² yr⁻¹) are located in the south of the Lantau Island, south of Hong Kong Island, and middle, east



230

235



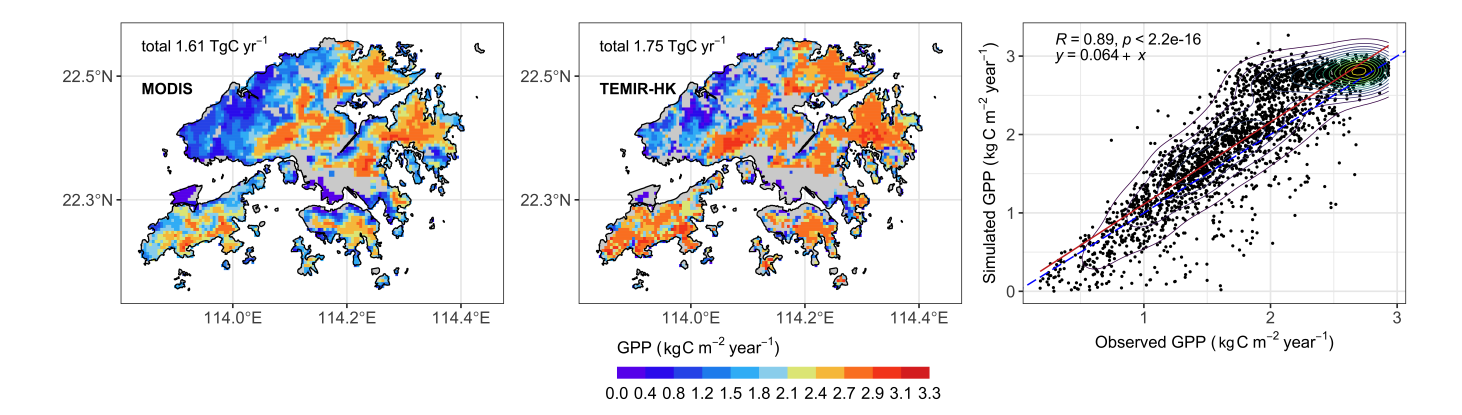


Figure 3. Spatial pattern of mean gross primary productivity (GPP) of Hong Kong from (a) observed MOD17A2HGFv6.1 product and (b) simulated Terrestrial Ecosystem Model in R (TEMIR-HK) for 2004–2018. (c) Spatial correlation between the observed and simulated GPP. Red solid line indicates the linear regression line, blue dashed line indicates 1:1 line. The coloured contours show the density of the points. The statistical metrics and the equation of the linear regression are annotated in the top-left corner of the plots.

and northeast of the New Territories. These regions are mainly dominated by broadleaf evergreen tropical trees (Figure 2) and are regarded as the country park areas in Hong Kong with dense vegetation. Meanwhile, lower GPP levels (0.8–1.8 kgC m⁻² yr⁻¹) are located in the northwest of the New Territories where the land cover is sparsely composed of grasses and needleleaf evergreen tropical trees (Figure 2). A spatial gradient is not observed as latitudinal variation is minimal over the study region. The magnitude of GPP in the broadleaf evergreen tree-dominated region is comparable to the average GPP at low latitudes (0–20° N) as estimated in Yu et al. (2014), whereas the average GPP over the entire Hong Kong is 1.51 kgC m⁻² yr⁻¹, which is also comparable to the estimated value in the East Asian monsoon region.

Over the course of the 15-year period, Hong Kong's total GPP increased by 6.8 %, from 1.46 TgC yr⁻¹ in 2004, to 1.56 TgC yr⁻¹ in 2018. The annual mean total GPP estimated by TEMIR-HK is 1.75 TgC yr⁻¹. Similar to the spatial patterns, the annual mean total GPP from TEMIR-HK is 8.7 % higher than MODIS GPP that is 1.61 TgC yr⁻¹. M-K test result shows a significant temporal trend in GPP (t = 0.562, p < 0.05) of 0.0115 ± 0.0028 TgC yr⁻². For the proposed drivers, [CO₂], LAI as well as temperature show statistically significant trends ([CO₂]: t = 1, p < 0.05; LAI: t = 0.657, p < 0.05; Temperature: t = 0.524, p < 0.05) of 2.3 ppm yr⁻¹, 0.0095 m² m⁻² yr⁻¹ and 0.054 °C yr⁻¹ respectively. Whereas for [O₃], the trend is statistically insignificant at a rate of 0.39 ppb yr⁻¹.

The GPP trend in Hong Kong exhibits a heterogeneous spatial pattern as depicted in Fig. 4. The pattern is distinct from the spatial GPP distribution presented above. In general, the magnitude of GPP trend of 80 % vegetated area lies within the range of $0.6-26.2~{\rm gC~m^{-2}~yr^{-2}}$. Large clusters of high GPP trend (>45 gC m⁻² yr⁻²) are spotted in west New Territories and north Lantau Island. Some scattered 9 % of the vegetated area experiences a negative trend up to $-25~{\rm gC~m^{-2}~yr^{-2}}$, yet none of these trends are statistically significant. Despite the fact that total GPP manifests a significant trend, only 39.6 % of vegetated area experience significant GPP increment (p < 0.05). Yet, the vegetation therein contributes to 69.2 % of the total GPP trend. We





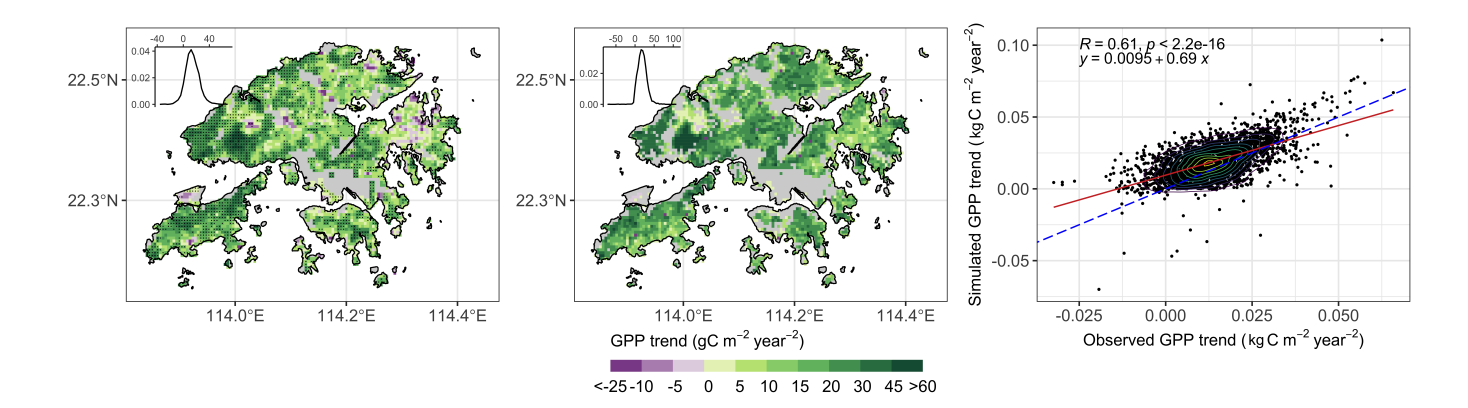


Figure 4. Spatial pattern of mean gross primary productivity (GPP) trends of Hong Kong from (a) observed MOD17A2HGFv6.1 product and (b) simulated Terrestrial Ecosystem Model in R (TEMIR-HK) for 2004-2018. (c) Spatial correlation between the observed and simulated GPP trends. Red solid line indicates the linear regression line, blue dashed line indicates 1:1 line. The coloured contours show the density of the points. The statistical metrics and the equation of the linear regression are annotated at the top-left corner of the plot.

further calculated the standard deviation of the linearly detrended annual GPP. Large IAV ($>0.2 \text{ kgC m}^{-2} \text{ yr}^{-1}$) happen at east New Territories, south Hong Kong Island and north and west Lantau Island. Large area of the northwest New Territories shows smaller IAV ($<0.1 \text{ kgC m}^{-2} \text{ yr}^{-2}$) (Figure S2).

3.2 Model evaluation

245

250

255

We further investigated whether the model simulations capture the same spatiotemporal characteristics as the observations. Some grid cells, depicted as grey areas in Figure 4b, mainly urban areas, were not simulated due to unavailable LAI data or low vegetation coverage (PFT fraction < 1 %). Here we assume that urban vegetation is negligible in contributing to the total GPP over the whole region given the extensive forests in the countryside. Overall, TEMIR-HK could reproduce a consistent spatial pattern on a par with the observations: high and low GPP regions are clearly distinguished (Fig. 3b). Spatial correlation between MODIS GPP and TEMIR-HK GPP shows a satisfactory correlation coefficient of 0.89 (Fig. 3c). However, TEMIR-HK slightly overestimates GPP over the whole region. The correlation shows a slight overestimation for simulated GPP on lower GPP levels, and the discrepancy widens at higher levels. Particularly, observed low-level GPP regions in the west Lantau Island are estimated to produce high GPP. Simulated time series of total GPP over Hong Kong shows a consistent pattern with satellite observations, with a correlation coefficient of 0.85. We also assessed the spatial pattern of GPP trend and IAV simulated by TEMIR-HK. The spatial correlation between the simulated and observed GPP trends demonstrates a good correlation coefficient of 0.61, although an overestimation of the rising trend by TEMIR-HK is evident (Fig. 4c). The two clusters of outstandingly strong GPP trends were also captured by the simulation. The correlation coefficient in the case of IAV is 0.34, implicating the model performs only fairly in estimated IAV (Fig. S3).





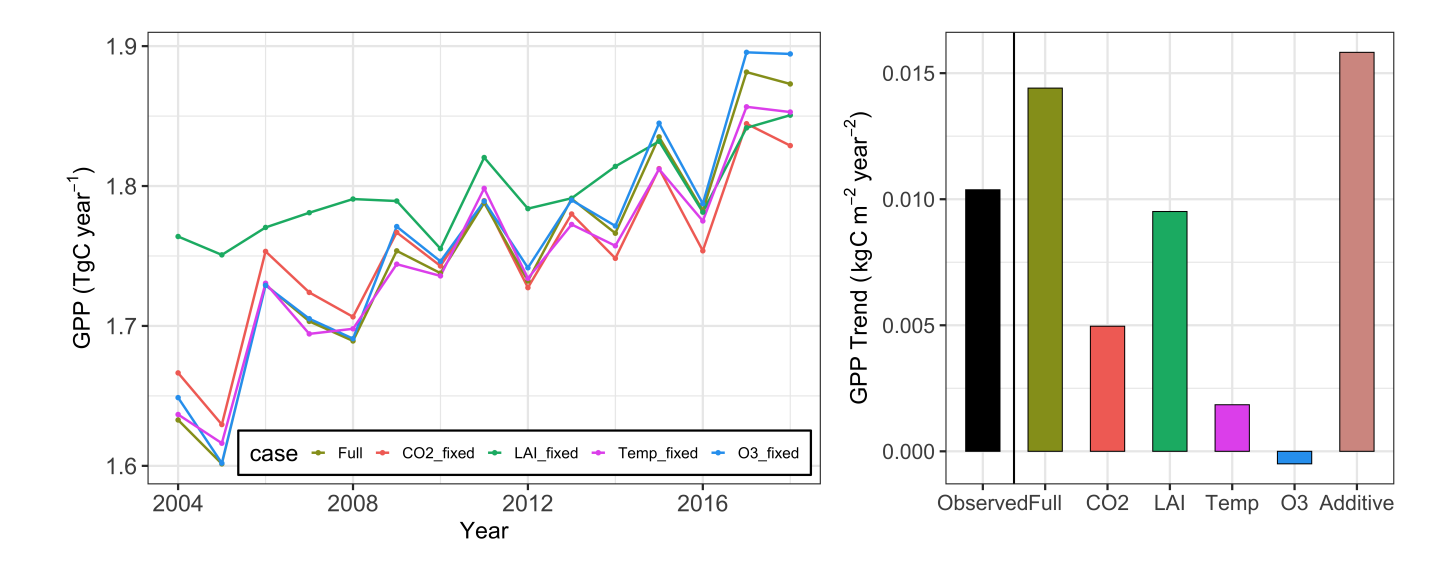


Figure 5. Time series of annual total gross primary production (GPP) for all factorial simulations described in Table 1. (b) Spatial mean GPP trends attributed to climatic and environmental factors, along with the additive trend resulting from the combined effect of these factors. The isolated black-coloured bar is the observed GPP trend calculated from MOD17A2HGFv6.1 product.

3.3 Total GPP trend responses to climatic and environmental factors

Here we show the attribution analysis results from the factorial simulations. Figure 5a shows the time series of annual total GPP from all factorial simulations. All cases show increasing yet interannually varying pattern. The GPP time series for 〈LAI _fixed〉 has notable difference in the pattern comparing with other cases. We applied M-K test to the total annual GPP time series to evaluate the level of significance. All of the simulations show significant trends with p-value smaller than 0.005. As Fig. 5b shows, GPP increases steadily with a positive trend of +0.0159 kgC m⁻² yr⁻². The trend of MODIS GPP is 11.0 % less than that of 〈Full〉 GPP. We decomposed the trend with factorial simulations by subtracting 〈fixed〉 GPP from 〈Full〉 GPP, followed by linear regression. The statistical metrics are shown in Table S1. LAI dominates the trend by +0.0134 TgC yr⁻², alongside with temperature and [CO₂] that also contribute to the increasing GPP. [O₃] is the only variable that is attributed to a negative trend. The additive (CO₂ + LAI + Temperature + O₃ effects) trend is slightly higher (+12.4 %) than the full trend, indicating some interactive effects might have offset part of the joint positive trend.

We conducted a simple sensitivity analysis by dividing the GPP trends induced by the proposed drivers by their own trends (Table 2). Rising [CO₂], LAI and temperature have positive effects on GPP; mildly rising [O₃] has a weak negative effect on GPP. In the period of 2004–2018, for every 10 ppm of [CO₂], 0.1 m² m⁻² of LAI, 1 °C of temperature and 1 ppb of [O₃], GPP changes for 23.8, 111, 37.8 and –1.41 gC m⁻² yr⁻¹ respectively. The increase in [CO₂], LAI, temperature and O₃ from 2004 to 2018 results in the increment of GPP by 0.091, 0.174, 0.034 and –0.009 TgC yr⁻¹ respectively.



285



Table 2. Annual trends (unit per year) and the gross primary productivity (GPP) trends (gC m⁻² yr⁻²) induced by atmospheric CO₂ concentration ([CO₂]), leaf area index (LAI), surface air temperature (Temp), ambient O₃ concentration ([O₃]). Sensitivities (gC m⁻² yr⁻¹ per unit) are the changes in GPP per unit change of the environmental variables. Single asterisk (*) indicates that the trend is significant under the non-parametric Mann-Kendall trend test (p < 0.05).

	Trend	Induced GPP trend	Sensitivity
[CO ₂] (10 ppm)	0.23 *	5.48 *	23.8
LAI (0.1 m ² m ⁻²)	0.095 *	10.5 *	110
Temp (1 °C)	0.0540 *	2.04 *	37.8
[O ₃] (1 ppb)	0.39	-0.548 *	-1.41

275 3.4 Total GPP IAV responses to climatic and environmental factors

The IAV of GPP in response to the proposed drivers are depicted in Fig. 6. We analysed the influence of the proposed drivers on IAV of GPP at two dimensions: magnitude through variance and linearity through correlation. Quantitatively, the SD of GPP induced by $[CO_2]$, LAI, temperature and $[O_3]$ are 2.45×10^{-3} , 2.77×10^{-2} , 8.44×10^{-3} and 6.74×10^{-3} TgC yr⁻¹ respectively. LAI induced the largest IAV on GPP by a magnitude of 1 compared to [CO₂], temperature and [O₃]. We also conducted Pearson correlation test between IAV of GPP (solid lines in Fig. 6) and the normalized IAV of the proposed drivers (dashed lines). While TEMIR-HK is a process-based model simulating instantaneous vegetation responses, the correlation coefficients do not imply the relationships between the environmental factors and GPP, as they are already supported by the well-established ecophysiological processes included in the model. Instead, they serve as indicators of the degree of linearity to which the environmental factors influence GPP. A higher magnitude in the Pearson coefficient indicates a more linear influence between the IAV of environmental factor and IAV of GPP, vice versa. [CO₂] has almost negligible influence on IAV of GPP in comparison with other drivers, which could be explained by the linearity of the time evolution of [CO₂] over the study period. The correlation coefficient is 0.94 with a high level of significance, suggesting that the [CO₂] has minimal yet linear influence on IAV of GPP. LAI dominates the variance among the other factors, and the correlation coefficient is 0.98 with a high level of significance, which suggests a strong and linear influence on IAV of GPP. Temperature has a moderate influence on IAV of GPP in the context of variance, and the relationship is more nonlinear compared to the former two drivers as the correlation is insignificant (p > 0.05) and the coefficient is 0.48. $[O_3]$ has a similar magnitude of influence on IAV of GPP, however, the relationship is nonlinear as the correlation coefficient is only -0.33.

3.5 Leaf area index dominates GPP trend and interannual variability

CO₂ fertilization effect is said to be the dominant driver of increasing global GPP from model simulations and satellite-based products, albeit having the largest uncertainty in the magnitude of effect (Walker et al., 2021; Yang et al., 2022). A recent study focusing on Yangtsz River Delta in China suggests that in the regions with significant greening, the joint effect of CO₂ fertilization effect on LAI and land management could result in the LAI variations, and in turn dominate the variations of



305



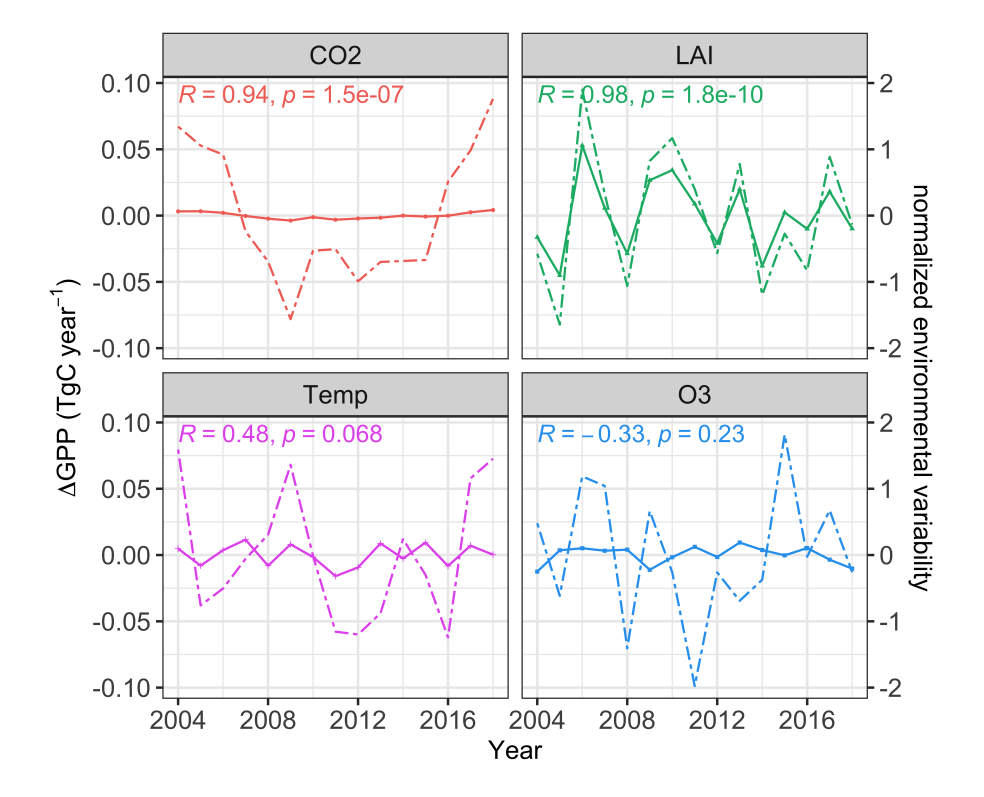


Figure 6. Interannual variability of gross primary production (GPP) influenced by environmental factors, as depicted by the solid lines. The corresponding normalized interannual variability of the environmental factors are depicted as dashed lines. Statistical metrics of Pearson correlation between the GPP interannual variability and environmental factor variability are presented on the top-left corner of the plots.

GPP (Chen et al., 2023a). Sensitivity analysis in that study showed that LAI increment of 0.1 would lead to a higher GPP increase than that of atmospheric [CO₂] increment of 10 ppm. From our results, LAI explains the majority of the annual trend of GPP and IAV of GPP, and it is also the largest contributing factor to IAV of GPP in terms of magnitude and directness. Our sensitivity analysis also shows that the effect on GPP for every LAI increment of 0.1 m² m⁻² is almost five times that for every [CO₂] increment of 10 ppm. This aligns with Chen et al. (2023a) that the effect of LAI variations determines the variations of GPP. Lower contribution from the climatic and environmental factors from our results only reflects their direct roles on leaf-level GPP.

Indeed, LAI is a composite result integrating indirect climatic and environmental effects and direct human-induced effects on canopy structure via forest management. Rising [CO₂] is suggested to be the dominant driver of growing-season integrated LAI trend in South China (Zhu et al., 2016). Study by Chen et al. (2023b) reported that the indirect effect of increased [CO₂] accounts for 18.4 % of the total environmental effects on GPP. At the same time, rising temperatures have resulted in advanced leaf phenology in spring over the recent decades (Gu et al., 2022; Piao et al., 2015). Here we propose two more factors that could have possibly contributed to LAI-associated GPP trend. First, there is a significant growth in LAI in winter (December



325

335

340



to February) over the years (Figure S3). There are overall increments in LAI for all seasons, but the winter increments are much more significant. The winter increases in LAI promote a smaller yet noteworthy level of photosynthesis compared to summertime ones. The observational study of Tan et al. (2012) reported that even in cold winters, subtropical evergreen forests could maintain continuously high levels of photosynthesis. Second, there has been a rapid growth of forests in some particular regions via active tree replanting. Both observations and model simulations show two clusters of large GPP trend, and LAI of the two clusters also shows more than 90 % increment during the 15-year period (Figure S1). Although the magnitude of LAI remains at a moderate level (<3 m² m²), the percentage increase in LAI is large enough to support the total GPP trend, as mentioned in Sect. 3.1 that 39.6 % of vegetated area experiencing significant GPP increment contribute to 69.2 % of the total GPP trend, and that includes the two clusters of strong GPP trends. The one cluster in west New Territories (part of the Tai Lam Country Park) experienced a massive wildfire in 2006, burning more than 66000 plants. Aggressive tree planting exercises were carried out to rehabilitate the areas damaged by the wildfire (Agriculture, Fisheries and Conservation Department, 2007). By using canopy height model, Zhang et al. (2024) showed evidence of recovery in 44.9 % of Hong Kong's vegetated area. The study highlighted the superior benefits of active restoration over natural regeneration. The above suggests that small-scale forest management supplemented by fertilization could play a vital role in forest regrowth, even influencing the total GPP trend for the entire region.

On the ecosystem scale, there could be substantial and more rapid changes in LAI as it could also be influenced by fertility, management treatment and wildfire disturbances, on top of climatic and PFT categorization on regional scale. Hong Kong government initiated the PEP programme in 2009, which includes thinning of ageing exotic tree species, predominantly Acacia species, and replanting of native tree seedlings. In 2022, about 2700 exotic trees were removed and more than 27000 native tree seedlings were replanted under the PEP. These Acacia species are suggested to limit plant growth through soil constraint and reduce ecosystem services (Lee et al., 2021). The replantation of vegetation under PEP could contribute to increasing LAI and consequently GPP, although the extent is uncertain. Rising LAI generally first result in an almost linear increase in GPP, but as LAI increases further, the dense leaves would attenuate more solar radiation, which would later become saturated at a certain LAI threshold. The growth rate of GPP would thus decline when LAI surpasses that threshold (Zhao et al., 2021). The highly linear relationship between IAV of GPP and LAI illustrated in Sect. 1.3.5 also suggests that the annual LAI has not yet reach the saturation threshold proposed by Zhao et al. (2021), who described the relation as a power function, although seasonally high LAI might have surpassed the threshold.

At the same time, studies have also showed that large inconsistencies between LAI from models and from satellite products could lead to significant uncertainties in GPP estimates (Chen et al., 2023a; Yang et al., 2022). Winkler et al. (2021) suggested that CO₂ fertilization effect on greening is only dominant in temperate forests, cool arid grasslands and the Australian shrublands, and in the tropical forests the effect is compensated by the browning caused by CO₂-induced climate change. It is therefore important to ensure the quality of LAI used as model input since that LAI is both a determinant and a consequence of important processes in canopy dynamics (Parker, 2020).



345

350

355

360

365

370

375



4 Conclusions and Implications

We examined forest GPP and its changes in Hong Kong within a recent 15-year period. We found that high GPP regions are broadleaf evergreen tree-dominated country park areas, where GPP is comparable to the level in tropical zones. Total GPP has been increasing with a significant trend, whereby the increases are the most concentrated in only around two-fifth of the vegetated areas that show significant increase in GPP. One of the two clusters showing large GPP trends experienced wildfire disturbances and aggressive tree replanting afterward, suggesting that small-scale forest management strategies can influence the GPP trend of the entire metropolitan city. Despite the dominance of broadleaf evergreen trees in Hong Kong, needleleaf evergreen temperate trees are actually the largest contributor to the GPP trend as a large fraction of their abundance is located in that cluster. We further explored the issues with attribution analysis utilizing our process-based model. Model simulations showed satisfactory results in reproducing the spatial GPP and its trend, albeit with very minor overestimation in general. The attribution analysis showed that LAI and [CO₂] contribute to the majority of the positive GPP trend in Hong Kong, while positive surface temperature effect is almost compensated by the negative O₃ and interactive effects. The interannual variability of GPP is also dominated by LAI, as it induces large and direct effect on GPP. On the other hand, the temperature and O₃ effects are much more nonlinear, and have moderate influence on GPP.

In our study we forced the model with prescribed satellite-based LAI dataset, which was model limitation but also in effect simplified the representation of land cover and land use change. The downside is the inability to decipher whether the overall increases in LAI in Hong Kong (Figure S1) are attributable to biophysical factors such as CO₂ fertilization and/or anthropogenic factors such as the active replacement of old forests as an ecological restoration strategy by the Hong Kong Government. Currently, there is no research on the effectiveness of the PEP, e.g., by quantifying the number of successfully replanted trees, or the changes in vegetation dynamics including the growth of understory canopies. This limits our research from examining the changes in potential productivity of vegetation induced by forest management. More attention should be paid to the effects of forest management and land cover change on the time evolution of LAI at such a limited spatial scale of the study. Future research may also focus on whole ecosystem modelling in Hong Kong, in order to disentangle the direct human effects and indirect climatic and environmental effects on leaf phenology, canopy structure, vegetation distribution, and the resulting integrated GPP.

Most land models including TEMIR-HK classify vegetation into a reduced set of similarly "behaving" plant types in terms of their ecosystem functions. However, subtropical tree species were observed to exhibit species-specific responses to rising temperature. The study from Li et al. (2016) showed certain species demonstrate a positive relationship between photosynthesis and variations in leaf temperature, whereas one particular species displays a decreased net photosynthetic rate in a warmer environment. Three species in the same study experienced increases in the proxies of leaf photosynthesis, namely maximum rate of Rubisco carboxylation (V_{cmax}) and the maximum rate of photosynthetic electron transport (J_{max}), which aligns with the model proposed by Farquhar et al. (1980). However, contradicting results were also observed in the other two species. It remains uncertain whether the current parameterization of broadleaf evergreen tropical trees could accurately represent the temperature responses and acclimation of the biodiverse subtropical forest ecosystems in Hong Kong.



380

385

390

395

405

410



To have a better representation of vegetation functionalities in a specific ecosystem, it is essential to incorporate local measurements of plant traits into models. The current version of TEMIR-HK calculates $V_{\rm cmax}$ at 25 °C in relation to prescribed PFT-specific leaf nitrogen concentration, fraction of leaf nitrogen in Rubisco and specific leaf area. Leaf-level $V_{\rm cmax25}$ can be derived from leaf-level gas exchange measurements and this approach has been widely adopted as the primary method $V_{\rm cmax25}$ estimation (Stinziano et al., 2017). A recent study (Liu et al., 2023) proposed an alternative and rapid method for estimating $V_{\rm cmax25}$ using canopy-level imaging spectroscopy to address challenges in sampling and measuring this trait in tall trees within natural forest ecosystems and remote regions including subtropical forests. This opens up an opportunity to collect mass $V_{\rm cmax25}$ data samples and obtain locally measured representative plant traits for ecosystem modelling in Hong Kong in the future.

Land cover change is not comprehensively represented in this study. A more complete representation of land cover change should include changes in both LAI, which represents canopy structure, and PFT fraction, which represents vegetation distribution. Currently, a dynamic vegetation or land cover change map is lacking in Hong Kong, and thus a constant land cover map was adopted. The high resolution 30 m FROM-GLC map is only available for 2015 and the effect of land cover change is only implicitly represented by the change in LAI in the case where deforestation and reforestation take place. Future developments in land cover change maps in Hong Kong would benefit our model simulation to take the effect fully into account.

Being one of the most populated city in the world, Hong Kong has announced targets for the city to attain carbon neutrality by 2050, with an interim goal of cutting carbon emissions by 50 % before 2035 relative to 2005 levels (The Government of the Hong Kong Special Administrative Region, 2021). In October 2021, the government unveiled Hong Kong's Climate Action Plan 2050, detailing four key decarbonization strategies: "net-zero electricity generation", "energy efficiency and sustainable buildings", "environmentally friendly transportation", and "waste minimization". These strategies, along with interim targets, are designed to pave the way for Hong Kong to achieve carbon neutrality by 2050. In addition to cutting carbon emissions, utilizing land carbon sink has been heralded as a complementary approach to achieve the goal.

According to governmental data, within the study period, the CO₂-equivalent annual mean of the total GHG emissions in Hong Kong was around 11.72 TgC yr⁻¹ (https://cnsd.gov.hk/wp-content/uploads/2025/04/Data-Tables_2023_AR5_per-capita_intensity-r2_clean.pdf, last access: 6 June 2025). Our estimated GPP of 1.75 TgC yr⁻¹ is about 15.0 % than that of the total GHG emissions from production sectors, indicating that productivity of Hong Kong's terrestrial ecosystems play a small yet indispensable role in achieving carbon neutrality. Noting that GPP is only a proxy of the actual carbon uptake for the ecosystem (net ecosystem productivity, NEP), the net uptake that contributes as carbon sink is even smaller than this 15 %. Given the extensive existing vegetation coverage in Hong Kong (~70 %), reforestation measures would not be beneficial toward neutrality targets as it is difficult to further increase the greening area. Instead, the focus should be on preserving existing ecosystems—any further loss in land carbon sink is another burden to the mitigation strategies. Most importantly, it highlights that both the public and the government need to act more progressively to cut anthropogenic carbon emissions, as the terrestrial ecosystems only have a limited potential to contribute to carbon neutrality in Hong Kong.

We emphasize the importance of the combined effect of indirect climatic and environmental conditions and direct forest management as reflected by LAI, since it dominates both the trend and interannual variability of our studies, alongside previous literature stating that discrepancies in LAI datasets cause diverse GPP estimation. There are needs for future work in





quantitative description on land cover change in Hong Kong, full ecosystem modelling and localized vegetative behaviour parameterization.

415 Code and data availability. Model output data used for analysis and plotting will be provided upon request. The vanilla Terrestrial Ecosystem Model in R (version 1.0) source code is licensed and publicly available in the following repository: https://doi.org/10.5281/zenodo.8215332 (Tai and Yung, 2023); as well as on GitHub: https://github.com/amospktai/TEMIR (last access: 1 Aug 2025). The modified model source code for Hong Kong will be provided upon request.

Author contributions. APKT designed the study and supervised the writing of the paper. HCHL conducted model simulations, analysed the
 results, and wrote the draft with the assistance of JTWL and DKCT. MSW and JW assisted in the interpretation of the results. All authors contributed to the discussion and improvement of the paper.

Competing interests. The contact author has declared that none of the authors has any competing interests.

Acknowledgements. This work was supported by the National Natural Science Foundation of China (NSFC) Research Grants Council (RGC) Joint Research Scheme (reference #: N_CUHK440/20, 42061160479) and the Collaborative Research Fund (reference #: C5062-21GF) from RGC. APKT and JW were supported by the Innovation and Technology Fund (funding support to the State Key Laboratory of Agrobiotechnology). MSW thanks the funding support by the General Research Fund (Grant No. 15603923 and 15609421), and the Collaborative Research Fund (Grant No. C5062-21GF) from the Research Grants Council, Hong Kong, China.





References

- Agriculture, Fisheries and Conservation Department: Annual Report 2006-2007, Country & Marine Parks, Tech. rep., https://www.afcd.gov. hk/misc/download/annualreport2007/eng/country.html, 2007.
 - Agriculture, Fisheries and Conservation Department: Annual Report 2022-2023, Country & Marine Parks, Tech. rep., https://www.afcd.gov. hk/misc/download/annualreport2023/en/country-and-marine-parks, 2023.
 - Ainsworth, E. A. and Rogers, A.: The Response of Photosynthesis and Stomatal Conductance to Rising [CO2]: Mechanisms and Environmental Interactions, Plant Cell Environ, 30, 258–270, https://doi.org/10.1111/j.1365-3040.2007.01641.x, 2007.
- Berry, J. and Bjorkman, O.: Photosynthetic Response and Adaptation to Temperature in Higher Plants, Annual Review of Plant Biology, 31, 491–543, https://doi.org/10.1146/annurev.pp.31.060180.002423, 1980.
 - Chan, E. P. Y., Fung, T., and Wong, F. K. K.: Estimating Above-Ground Biomass of Subtropical Forest Using Airborne LiDAR in Hong Kong, Sci Rep, 11, 1751, https://doi.org/10.1038/s41598-021-81267-8, 2021.
- Chen, C., Park, T., Wang, X., Piao, S., Xu, B., Chaturvedi, R. K., Fuchs, R., Brovkin, V., Ciais, P., Fensholt, R., Tommervik, H., Bala, G.,
 Zhu, Z., Nemani, R. R., and Myneni, R. B.: China and India Lead in Greening of the World through Land-Use Management, Nat Sustain,
 2, 122–129, https://doi.org/10.1038/s41893-019-0220-7, 2019.
 - Chen, X., Cai, A., Guo, R., Liang, C., and Li, Y.: Variation of Gross Primary Productivity Dominated by Leaf Area Index in Significantly Greening Area, Journal of Geographical Sciences, 33, 1747–1764, https://doi.org/10.1007/s11442-023-2151-5, 2023a.
- Chen, Y., Zhu, Z., Zhao, W., Li, M., Cao, S., Zheng, Y., Tian, F., and Myneni, R. B.: The Direct and Indirect Effects of the Environmental Factors on Global Terrestrial Gross Primary Productivity over the Past Four Decades, Environmental Research Letters, 19, https://doi.org/10.1088/1748-9326/ad107f, 2023b.
 - Cheng, W., Dan, L., Deng, X., Feng, J., Wang, Y., Peng, J., Tian, J., Qi, W., Liu, Z., Zheng, X., Zhou, D., Jiang, S., Zhao, H., and Wang, X.: Global Monthly Gridded Atmospheric Carbon Dioxide Concentrations under the Historical and Future Scenarios, Sci Data, 9, 83, https://doi.org/10.1038/s41597-022-01196-7, 2022.
- Cui, E., Huang, K., Arain, M. A., Fisher, J. B., Huntzinger, D. N., Ito, A., Luo, Y., Jain, A. K., Mao, J., Michalak, A. M., Niu, S., Parazoo, N. C., Peng, C., Peng, S., Poulter, B., Ricciuto, D. M., Schaefer, K. M., Schwalm, C. R., Shi, X., Tian, H., Wang, W., Wang, J., Wei, Y., Yan, E., Yan, L., Zeng, N., Zhu, Q., and Xia, J.: Vegetation Functional Properties Determine Uncertainty of Simulated Ecosystem Productivity: A Traceability Analysis in the East Asian Monsoon Region, Global Biogeochemical Cycles, 33, 668–689, https://doi.org/10.1029/2018gb005909, 2019.
- Donohue, R. J., Roderick, M. L., McVicar, T. R., and Farquhar, G. D.: Impact of CO2 Fertilization on Maximum Foliage Cover across the Globe's Warm, Arid Environments, Geophysical Research Letters, 40, 3031–3035, https://doi.org/10.1002/grl.50563, 2013.
 - Dudgeon, D. and Corlett, R.: Hills and Streams: An Ecology of Hong Kong, Hong Kong University Press, ISBN 978-962-209-357-7, http://www.jstor.org/stable/j.ctt2jc0hg, 1994.
- Farquhar, G. D., von Caemmerer, S., and Berry, J. A.: A Biochemical Model of Photosynthetic CO2 Assimilation in Leaves of C3 Species,
 460 Planta, 149, 78–90, https://doi.org/10.1007/BF00386231, 1980.
 - Fernández-Martínez, M., Sardans, J., Chevallier, F., Ciais, P., Obersteiner, M., Vicca, S., Canadell, J. G., Bastos, A., Friedlingstein, P., Sitch, S., Piao, S. L., Janssens, I. A., and Peñuelas, J.: Global Trends in Carbon Sinks and Their Relationships with CO2 and Temperature, Nature Climate Change, 9, 73–79, https://doi.org/10.1038/s41558-018-0367-7, 2018.





- Franz, M. and Zaehle, S.: Competing Effects of Nitrogen Deposition and Ozone Exposure on Northern Hemispheric Terrestrial Carbon
 Uptake and Storage, 1850–2099, Biogeosciences, 18, 3219–3241, https://doi.org/10.5194/bg-18-3219-2021, 2021.
 - Friedlingstein, P., O'Sullivan, M., Jones, M. W., Andrew, R. M., Bakker, D. C. E., Hauck, J., Landschützer, P., Le Quéré, C., Luijkx, I. T., Peters, G. P., Peters, W., Pongratz, J., Schwingshackl, C., Sitch, S., Canadell, J. G., Ciais, P., Jackson, R. B., Alin, S. R., Anthoni, P., Barbero, L., Bates, N. R., Becker, M., Bellouin, N., Decharme, B., Bopp, L., Brasika, I. B. M., Cadule, P., Chamberlain, M. A., Chandra, N., Chau, T.-T.-T., Chevallier, F., Chini, L. P., Cronin, M., Dou, X., Enyo, K., Evans, W., Falk, S., Feely, R. A., Feng, L., Ford, D. J.,
- Gasser, T., Ghattas, J., Gkritzalis, T., Grassi, G., Gregor, L., Gruber, N., Gürses, Ö., Harris, I., Hefner, M., Heinke, J., Houghton, R. A., Hurtt, G. C., Iida, Y., Ilyina, T., Jacobson, A. R., Jain, A., Jarníková, T., Jersild, A., Jiang, F., Jin, Z., Joos, F., Kato, E., Keeling, R. F., Kennedy, D., Klein Goldewijk, K., Knauer, J., Korsbakken, J. I., Körtzinger, A., Lan, X., Lefèvre, N., Li, H., Liu, J., Liu, Z., Ma, L., Marland, G., Mayot, N., McGuire, P. C., McKinley, G. A., Meyer, G., Morgan, E. J., Munro, D. R., Nakaoka, S.-I., Niwa, Y., O'Brien, K. M., Olsen, A., Omar, A. M., Ono, T., Paulsen, M., Pierrot, D., Pocock, K., Poulter, B., Powis, C. M., Rehder, G., Resplandy, L.,
- Robertson, E., Rödenbeck, C., Rosan, T. M., Schwinger, J., Séférian, R., Smallman, T. L., Smith, S. M., Sospedra-Alfonso, R., Sun, Q., Sutton, A. J., Sweeney, C., Takao, S., Tans, P. P., Tian, H., Tilbrook, B., Tsujino, H., Tubiello, F., van der Werf, G. R., van Ooijen, E., Wanninkhof, R., Watanabe, M., Wimart-Rousseau, C., Yang, D., Yang, X., Yuan, W., Yue, X., Zaehle, S., Zeng, J., and Zheng, B.: Global Carbon Budget 2023, Earth System Science Data, 15, 5301–5369, https://doi.org/10.5194/essd-15-5301-2023, 2023.
- Gong, P., Wang, J., Yu, L., Zhao, Y., Zhao, Y., Liang, L., Niu, Z., Huang, X., Fu, H., Liu, S., Li, C., Li, X., Fu, W., Liu, C., Xu, Y., Wang, X.,
 Cheng, Q., Hu, L., Yao, W., Zhang, H., Zhu, P., Zhao, Z., Zhang, H., Zheng, Y., Ji, L., Zhang, Y., Chen, H., Yan, A., Guo, J., Yu, L., Wang, L., Liu, X., Shi, T., Zhu, M., Chen, Y., Yang, G., Tang, P., Xu, B., Giri, C., Clinton, N., Zhu, Z., Chen, J., and Chen, J.: Finer Resolution Observation and Monitoring of Global Land Cover: First Mapping Results with Landsat TM and ETM+ Data, International Journal of Remote Sensing, 34, 2607–2654, https://doi.org/10.1080/01431161.2012.748992, 2012.
- Gu, F., Zhang, Y., Huang, M., Tao, B., Guo, R., and Yan, C.: Effects of Climate Warming on Net Primary Productivity in China during 1961-2010, Ecol Evol, 7, 6736–6746, https://doi.org/10.1002/ece3.3029, 2017.
 - Gu, H., Qiao, Y., Xi, Z., Rossi, S., Smith, N. G., Liu, J., and Chen, L.: Warming-Induced Increase in Carbon Uptake Is Linked to Earlier Spring Phenology in Temperate and Boreal Forests, Nat Commun, 13, 3698, https://doi.org/10.1038/s41467-022-31496-w, 2022.
 - Hikosaka, K., Ishikawa, K., Borjigidai, A., Muller, O., and Onoda, Y.: Temperature Acclimation of Photosynthesis: Mechanisms Involved in the Changes in Temperature Dependence of Photosynthetic Rate, J Exp Bot, 57, 291–302, https://doi.org/10.1093/jxb/erj049, 2006.
- Huang, Y., Chen, Y., Castro-Izaguirre, N., Baruffol, M., Brezzi, M., Lang, A., Li, Y., Härdtle, W., von Oheimb, G., Yang, X., Liu, X., Pei, K., Both, S., Yang, B., Eichenberg, D., Assmann, T., Bauhus, J., Behrens, T., Buscot, F., Chen, X.-Y., Chesters, D., Ding, B.-Y., Durka, W., Erfmeier, A., Fang, J., Fischer, M., Guo, L.-D., Guo, D., Gutknecht, J. L. M., He, J.-S., He, C.-L., Hector, A., Hönig, L., Hu, R.-Y., Klein, A.-M., Kühn, P., Liang, Y., Li, S., Michalski, S., Scherer-Lorenzen, M., Schmidt, K., Scholten, T., Schuldt, A., Shi, X., Tan, M.-Z., Tang, Z., Trogisch, S., Wang, Z., Welk, E., Wirth, C., Wubet, T., Xiang, W., Yu, M., Yu, X.-D., Zhang, J., Zhang, S., Zhang, N., Zhou, H.-Z.,
- Zhu, C.-D., Zhu, L., Bruelheide, H., Ma, K., Niklaus, P. A., and Schmid, B.: Impacts of Species Richness on Productivity in a Large-Scale Subtropical Forest Experiment, Science, 362, 80–83, https://doi.org/10.1126/science.aat6405, 2018.
 - Kong, L., Shi, Z., and Chu, L. M.: Carbon Emission and Sequestration of Urban Turfgrass Systems in Hong Kong, Science of The Total Environment, 473–474, 132–138, https://doi.org/10.1016/j.scitotenv.2013.12.012, 2014.
- Lands Department: Hong Kong Geographic Data, https://www.landsd.gov.hk/en/resources/mapping-information/hk-geographic-data.html, 2024.



510

520

530

535



- Lee, C. H. Y., Tang, A. M. C., Lai, D. Y. F., Tai, A. P. K., Leung, A. S. L., Tao, D. K. C., Leung, F., Leung, S. S. M., Wu, C., Tong, S. C. S., and Ng, K. T. K.: Problems and Management of Acacia-Dominated Urban Forests on Man-Made Slopes in a Subtropical, High-Density City, Forests, 12, https://doi.org/10.3390/f12030323, 2021.
- Li, C., Gong, P., Wang, J., Zhu, Z., Biging, G. S., Yuan, C., Hu, T., Zhang, H., Wang, Q., Li, X., Liu, X., Xu, Y., Guo, J., Liu, C., Hackman, K. O., Zhang, M., Cheng, Y., Yu, L., Yang, J., Huang, H., and Clinton, N.: The First All-Season Sample Set for Mapping Global Land Cover with Landsat-8 Data, Sci Bull (Beijing), 62, 508–515, https://doi.org/10.1016/j.scib.2017.03.011, 2017.
 - Li, S., Liu, Y., Gao, Y., and Ao, Y.: Variations and Trends of Terrestrial NPP and Its Relation to Climate Change in the 10 CMIP5 Models, Journal of Earth System Science, 124, 395–403, https://doi.org/10.1007/s12040-015-0545-1, 2015.
 - Li, Y., Liu, J., Zhou, G., Huang, W., and Duan, H.: Warming Effects on Photosynthesis of Subtropical Tree Species: A Translocation Experiment along an Altitudinal Gradient, Sci Rep, 6, 24 895, https://doi.org/10.1038/srep24895, 2016.
 - Liu, J. and Lai, D. Y. F.: Subtropical Mangrove Wetland Is a Stronger Carbon Dioxide Sink in the Dry than Wet Seasons, Agricultural and Forest Meteorology, 278, https://doi.org/10.1016/j.agrformet.2019.107644, 2019.
- Liu, S., Yan, Z., Wang, Z., Serbin, S., Visser, M., Zeng, Y., Ryu, Y., Su, Y., Guo, Z., Song, G., Wu, Q., Zhang, H., Cheng, K. H.,
 Dong, J., Hau, B. C. H., Zhao, P., Yang, X., Liu, L., Rogers, A., and Wu, J.: Mapping Foliar Photosynthetic Capacity in Sub-Tropical
 and Tropical Forests with UAS-based Imaging Spectroscopy: Scaling from Leaf to Canopy, Remote Sensing of Environment, 293,
 https://doi.org/10.1016/j.rse.2023.113612, 2023.
 - Lloyd, J. and Farquhar, G. D.: Effects of Rising Temperatures and [CO2] on the Physiology of Tropical Forest Trees, Philos Trans R Soc Lond B Biol Sci, 363, 1811–7, https://doi.org/10.1098/rstb.2007.0032, 2008.
 - Lombardozzi, D., Levis, S., Bonan, G., and Sparks, J. P.: Predicting Photosynthesis and Transpiration Responses to Ozone: Decoupling Modeled Photosynthesis and Stomatal Conductance, Biogeosciences, 9, 3113–3130, https://doi.org/10.5194/bg-9-3113-2012, 2012.
 - Lombardozzi, D., Levis, S., Bonan, G., Hess, P. G., and Sparks, J. P.: The Influence of Chronic Ozone Exposure on Global Carbon and Water Cycles, Journal of Climate, 28, 292–305, https://doi.org/10.1175/jcli-d-14-00223.1, 2015.
 - Lu, G. Y. and Wong, D. W.: An Adaptive Inverse-Distance Weighting Spatial Interpolation Technique, Computers & Geosciences, 34, 1044–1055, https://doi.org/10.1016/j.cageo.2007.07.010, 2008.
- Medlyn, B. E., Duursma, R. A., Eamus, D., Ellsworth, D. S., Prentice, I. C., Barton, C. V. M., Crous, K. Y., De Angelis, P., Freeman, M., and Wingate, L.: Reconciling the Optimal and Empirical Approaches to Modelling Stomatal Conductance, Global Change Biology, 17, 2134–2144, https://doi.org/10.1111/j.1365-2486.2010.02375.x, 2011.
 - Pan, S., Tian, H., Dangal, S. R. S., Ouyang, Z., Tao, B., Ren, W., Lu, C., and Running, S.: Modeling and Monitoring Terrestrial Primary Production in a Changing Global Environment: Toward a Multiscale Synthesis of Observation and Simulation, Advances in Meteorology, 2014, 1–17, https://doi.org/10.1155/2014/965936, 2014.
 - Park Williams, A., Allen, C. D., Macalady, A. K., Griffin, D., Woodhouse, C. A., Meko, D. M., Swetnam, T. W., Rauscher, S. A., Seager, R., Grissino-Mayer, H. D., Dean, J. S., Cook, E. R., Gangodagamage, C., Cai, M., and McDowell, N. G.: Temperature as a Potent Driver of Regional Forest Drought Stress and Tree Mortality, Nature Climate Change, 3, 292–297, https://doi.org/10.1038/nclimate1693, 2012.
 - Parker, G. G.: Tamm Review: Leaf Area Index (LAI) Is Both a Determinant and a Consequence of Important Processes in Vegetation Canopies, Forest Ecology and Management, 477, https://doi.org/10.1016/j.foreco.2020.118496, 2020.
 - Piao, S., Tan, J., Chen, A., Fu, Y. H., Ciais, P., Liu, Q., Janssens, I. A., Vicca, S., Zeng, Z., Jeong, S. J., Li, Y., Myneni, R. B., Peng, S., Shen, M., and Penuelas, J.: Leaf Onset in the Northern Hemisphere Triggered by Daytime Temperature, Nat Commun, 6, 6911, https://doi.org/10.1038/ncomms7911, 2015.



570



- Reinhart, V., Hoffmann, P., Rechid, D., Böhner, J., and Bechtel, B.: High-Resolution Land Use and Land Cover Dataset for Regional Climate

 Modelling: A Plant Functional Type Map for Europe 2015, Earth Syst. Sci. Data, 14, 1735–1794, https://doi.org/10.5194/essd-14-17352022, 2022.
 - Requena Suarez, D., Rozendaal, D. M. A., De Sy, V., Phillips, O. L., Alvarez-Davila, E., Anderson-Teixeira, K., Araujo-Murakami, A., Arroyo, L., Baker, T. R., Bongers, F., Brienen, R. J. W., Carter, S., Cook-Patton, S. C., Feldpausch, T. R., Griscom, B. W., Harris, N., Herault, B., Honorio Coronado, E. N., Leavitt, S. M., Lewis, S. L., Marimon, B. S., Monteagudo Mendoza, A., Kassi N'dja, J., N'Guessan,
- A. E., Poorter, L., Qie, L., Rutishauser, E., Sist, P., Sonke, B., Sullivan, M. J. P., Vilanova, E., Wang, M. M. H., Martius, C., and Herold, M.: Estimating Aboveground Net Biomass Change for Tropical and Subtropical Forests: Refinement of IPCC Default Rates Using Forest Plot Data, Glob Chang Biol, 25, 3609–3624, https://doi.org/10.1111/gcb.14767, 2019.
 - Ryu, Y., Berry, J. A., and Baldocchi, D. D.: What Is Global Photosynthesis? History, Uncertainties and Opportunities, Remote Sensing of Environment, 223, 95–114, https://doi.org/10.1016/j.rse.2019.01.016, 2019.
- Scafaro, A. P., Posch, B. C., Evans, J. R., Farquhar, G. D., and Atkin, O. K.: Rubisco Deactivation and Chloroplast Electron Transport Rates Co-Limit Photosynthesis above Optimal Leaf Temperature in Terrestrial Plants, Nat Commun, 14, 2820, https://doi.org/10.1038/s41467-023-38496-4, 2023.
 - Schimel, D., Stephens, B. B., and Fisher, J. B.: Effect of Increasing CO2 on the Terrestrial Carbon Cycle, Proc Natl Acad Sci U S A, 112, 436–41, https://doi.org/10.1073/pnas.1407302112, 2015.
- Sitch, S., Cox, P. M., Collins, W. J., and Huntingford, C.: Indirect Radiative Forcing of Climate Change through Ozone Effects on the Land-Carbon Sink, Nature, 448, 791–794, https://doi.org/10.1038/nature06059, sitch scheme for modelling ozone damage "high" and "low" sensitivities are based on the sensitivities of individual plant species

 The parameters of grasses come from field measurements of wheat and potato, 2007.
- Stinziano, J. R., Morgan, P. B., Lynch, D. J., Saathoff, A. J., McDermitt, D. K., and Hanson, D. T.: The Rapid A-C(i) Response: Photosynthesis in the Phenomic Era, Plant Cell Environ, 40, 1256–1262, https://doi.org/10.1111/pce.12911, 2017.
 - Tai, A. P. K. and Yung, D. H. Y.: TEMIR v1.0 Public Release, Zenodo, https://doi.org/10.5281/zenodo.8215332, 2023.
 - Tai, A. P. K., Yung, D. H. Y., and Lam, T.: Terrestrial Ecosystem Model in R (TEMIR) Version 1.0: Simulating Ecophysiological Responses of Vegetation to Atmospheric Chemical and Meteorological Changes, Geoscientific Model Development, 17, 3733–3764, https://doi.org/10.5194/gmd-17-3733-2024, 2024.
- Tan, Z.-H., Zhang, Y.-P., Liang, N., Hsia, Y.-J., Zhang, Y.-J., Zhou, G.-Y., Li, Y.-L., Juang, J.-Y., Chu, H.-S., Yan, J.-H., Yu, G.-R., Sun, X.-M., Song, Q.-H., Cao, K.-F., Schaefer, D. A., and Liu, Y.-H.: An Observational Study of the Carbon-Sink Strength of East Asian Subtropical Evergreen Forests, Environmental Research Letters, 7, 044 017, https://doi.org/10.1088/1748-9326/7/4/044017, 2012.
 - Tang, Y., Li, T., Yang, X.-Q., Chao, Q., Wang, C., Lai, D. Y. F., Liu, J., Zhu, X., Zhao, X., Fan, X., Zhang, Y., Hu, Q., and Qin, Z.: Mango-GPP: A Process-Based Model for Simulating Gross Primary Productivity of Mangrove Ecosystems, Journal of Advances in Modeling Earth Systems, 15, https://doi.org/10.1029/2023ms003714, 2023.
 - Tao, K. C.: Measuring and Modeling Ozone-vegetation Interactions in Hong Kong: Implications for Ecosystem Services Provided by Subtropical Vegetation, Master's thesis, The Chinese University of Hong Kong, https://repository.lib.cuhk.edu.hk/en/item/cuhk-3121683, 2021
- The Government of the Hong Kong Special Administrative Region: Hong Kong's Climate Action Plan 2050, https://cnsd.gov.hk/wp-content/ 575 uploads/pdf/CAP2050_booklet_en.pdf, 2021.



595



- Twine, T. E. and Kucharik, C. J.: Climate Impacts on Net Primary Productivity Trends in Natural and Managed Ecosystems of the Central and Eastern United States, Agricultural and Forest Meteorology, 149, 2143–2161, https://doi.org/10.1016/j.agrformet.2009.05.012, 2009.
- Uddling, J., Hogg, A. J., Teclaw, R. M., Carroll, M. A., and Ellsworth, D. S.: Stomatal Uptake of O3 in Aspen and Aspen-Birch Forests under Free-Air CO2 and O3 Enrichment, Environ Pollut, 158, 2023–31, https://doi.org/10.1016/j.envpol.2009.12.001, 2010.
- Vahisalu, T., Puzõrjova, I., Brosché, M., Valk, E., Lepiku, M., Moldau, H., Pechter, P., Wang, Y. S., Lindgren, O., Salojärvi, J., Loog, M., Kangasjärvi, J., and Kollist, H.: Ozone-Triggered Rapid Stomatal Response Involves the Production of Reactive Oxygen Species, and Is Controlled by SLAC1 and OST1, Plant J, 62, 442–53, https://doi.org/10.1111/j.1365-313X.2010.04159.x, 2010.
 - Verbyla, D.: Browning Boreal Forests of Western North America, Environmental Research Letters, 6, https://doi.org/10.1088/1748-9326/6/4/041003, 2011.
- Walker, A. P., De Kauwe, M. G., Bastos, A., Belmecheri, S., Georgiou, K., Keeling, R. F., McMahon, S. M., Medlyn, B. E., Moore, D. J. P., Norby, R. J., Zaehle, S., Anderson-Teixeira, K. J., Battipaglia, G., Brienen, R. J. W., Cabugao, K. G., Cailleret, M., Campbell, E., Canadell, J. G., Ciais, P., Craig, M. E., Ellsworth, D. S., Farquhar, G. D., Fatichi, S., Fisher, J. B., Frank, D. C., Graven, H., Gu, L., Haverd, V., Heilman, K., Heimann, M., Hungate, B. A., Iversen, C. M., Joos, F., Jiang, M., Keenan, T. F., Knauer, J., Korner, C., Leshyk, V. O., Leuzinger, S., Liu, Y., MacBean, N., Malhi, Y., McVicar, T. R., Penuelas, J., Pongratz, J., Powell, A. S., Riutta, T., Sabot, M. E. B.,
- Schleucher, J., Sitch, S., Smith, W. K., Sulman, B., Taylor, B., Terrer, C., Torn, M. S., Treseder, K. K., Trugman, A. T., Trumbore, S. E., van Mantgem, P. J., Voelker, S. L., Whelan, M. E., and Zuidema, P. A.: Integrating the Evidence for a Terrestrial Carbon Sink Caused by Increasing Atmospheric CO(2), New Phytol, 229, 2413–2445, https://doi.org/10.1111/nph.16866, 2021.
 - Winkler, A. J., Myneni, R. B., Hannart, A., Sitch, S., Haverd, V., Lombardozzi, D., Arora, V. K., Pongratz, J., Nabel, J. E. M. S., Goll, D. S., Kato, E., Tian, H., Arneth, A., Friedlingstein, P., Jain, A. K., Zaehle, S., and Brovkin, V.: Slowdown of the Greening Trend in Natural Vegetation with Further Rise in Atmospheric CO2, Biogeosciences, 18, 4985–5010, https://doi.org/10.5194/bg-18-4985-2021, 2021.
 - Wittig, V. E., Ainsworth, E. A., and Long, S. P.: To What Extent Do Current and Projected Increases in Surface Ozone Affect Photosynthesis and Stomatal Conductance of Trees? A Meta-Analytic Review of the Last 3 Decades of Experiments, Plant Cell Environ, 30, 1150–62, https://doi.org/10.1111/j.1365-3040.2007.01717.x, 2007.
- Wu, Z., Dijkstra, P., Koch, G. W., PeÑUelas, J., and Hungate, B. A.: Responses of Terrestrial Ecosystems to Temperature and Precipitation Change: A Meta-analysis of Experimental Manipulation, Global Change Biology, 17, 927–942, https://doi.org/10.1111/j.1365-2486.2010.02302.x, 2011.
 - Yang, R., Wang, J., Zeng, N., Sitch, S., Tang, W., McGrath, M. J., Cai, Q., Liu, D., Lombardozzi, D., Tian, H., Jain, A. K., and Han, P.: Divergent Historical GPP Trends among State-of-the-Art Multi-Model Simulations and Satellite-Based Products, Earth System Dynamics, 13, 833–849, https://doi.org/10.5194/esd-13-833-2022, 2022.
- Yu, G., Chen, Z., Piao, S., Peng, C., Ciais, P., Wang, Q., Li, X., and Zhu, X.: High Carbon Dioxide Uptake by Subtropical Forest Ecosystems in the East Asian Monsoon Region, Proc Natl Acad Sci U S A, 111, 4910–5, https://doi.org/10.1073/pnas.1317065111, 2014.
 - Zhang, H., Lee, C. K. F., Law, Y. K., Chan, A. H. Y., Zhang, J., Gale, S. W., Hughes, A., Ledger, M. J., Wong, M. S., Tai, A. P. K., Hau, B. C. H., and Wu, J.: Integrating Both Restoration and Regeneration Potentials into Real-World Forest Restoration Planning: A Case Study of Hong Kong, Journal of Environmental Management, 369, 122 306, https://doi.org/10.1016/j.jenvman.2024.122306, 2024.
- Zhao, W., Tan, W., and Li, S.: High Leaf Area Index Inhibits Net Primary Production in Global Temperate Forest Ecosystems, Environ Sci Pollut Res Int, 28, 22 602–22 611, https://doi.org/10.1007/s11356-020-11928-0, 2021.
 - Zhu, Z., Piao, S., Myneni, R. B., Huang, M., Zeng, Z., Canadell, J. G., Ciais, P., Sitch, S., Friedlingstein, P., Arneth, A., Cao, C., Cheng, L., Kato, E., Koven, C., Li, Y., Lian, X., Liu, Y., Liu, R., Mao, J., Pan, Y., Peng, S., Peñuelas, J., Poulter, B., Pugh, T. A. M., Stocker,





B. D., Viovy, N., Wang, X., Wang, Y., Xiao, Z., Yang, H., Zaehle, S., and Zeng, N.: Greening of the Earth and Its Drivers, Nature Climate Change, 6, 791–795, https://doi.org/10.1038/nclimate3004, 2016.